Microporous and Mesoporous Materials 248 (2017) 204–213

Contents lists available at ScienceDirect

Microporous and Mesoporous Materials

journal homepage: www.elsevier.com/locate/micromeso

Insights into the aminothermal crystallization process of SAPO-34 and its comparison with hydrothermal system

Beibei Gao [a, b, 1], Dong Fan [a, b, 1], Lijing Sun [a, b], Hongyu An [c], Fengtao Fan [c], Shutao Xu [a], Peng Tian [a, **], Zhongmin Liu [a, *]

[a] National Engineering Laboratory for Methanol to Olefins, Dalian National Laboratory for Clean Energy, iChEM (Collaborative Innovation Center of Chemistry for Energy Materials), Dalian Institute of Chemical Physics, Chinese Academy of Sciences, Dalian 116023, PR China
[b] University of Chinese Academy of Sciences, Beijing 100049, PR China
[c] State Key Laboratory of Catalysis, Dalian Institute of Chemical Physics, Chinese Academy of Sciences, Dalian 116023, PR China

ARTICLE INFO

Article history:
Received 17 February 2017
Received in revised form
5 April 2017
Accepted 16 April 2017
Available online 18 April 2017

Keywords:
Molecular sieves
SAPO-34
Crystallization
Aminothermal synthesis
Characterization

ABSTRACT

Aminothermal synthesis reported by our group recently, in which organic amine is used as the solvent and template, could obviously enhance the solid yield and crystallization rate of SAPO-34 as compared with the corresponding hydrothermal one. Herein, aminothermal crystallization process of SAPO-34 is investigated to gain insights into this novel synthetic method by XRD, SEM, IR, UV-Raman and various solid-state NMR techniques. It is found that aminothermal environment facilitates the fast formation of a semicrystalline AlPO layered phase, which further promotes the quick activation of Al source. The lamellar phase, which is water-soluble and contains double 6-rings in the framework, could be stabilized by protonated triethylamine (TEA^+). SAPO-34 nucleates from the rearrangement of the double 6-rings in the layered phase through bond breaking, reforming and Si incorporation after heating at 160 °C for 3 h. For the hydrothermal process, the interaction between TEA^+ and inorganic species is weak and the formation of layered phase is retarded due to its high solubility in water. Correspondingly, the activation of Al source is slow and SAPO-34 appears after 24 h. This work demonstrates the importance of water concentration in the synthetic system, which may influence the formation of intermediate species and alter the crystallization process and rate.

1. Introduction

Zeolites are a family of microporous crystalline materials containing uniform pores and cavities of molecular dimensions that have been extensively employed as heterogeneous acid catalysts in petrochemistry and fine chemical industries [1–5]. Due to the industrial importance of zeolites and the academic interest in their structural complexity and diverse physicochemical properties, considerable efforts have been devoted to zeolite synthesis, in which one breakthrough was the discovery of silicoaluminophosphate (SAPO) molecular sieves with a broad range of structure types in 1984 [6,7]. Among SAPOs, SAPO-34 is one of the most significant members, which exhibits excellent catalytic performance in the methanol-to-olefins (MTO) reaction due to its moderate acid strength, small pore and ideal chabazite cages for the formation of polymethylbenzenium intermediates (active species in the MTO reaction) [8–14]. Hitherto, hydrothermal method is the primary strategy to synthesize SAPO-34 [15–19], together with other synthetic approaches such as dry-gel conversion [20–22] and solvent-free synthesis [23].

Novel synthetic methods, which may bring the opportunity to create new materials or known phases with specific properties, are always attractive in the field of molecular sieves [24,25]. In our previous work, a novel aminothermal synthesis route, in which organic amines are used as both the solvent and template, has been developed for the synthesis of SAPO molecular sieves [26,27]. It was demonstrated that the aminothermal method was an effective route to synthesize SAPO molecular sieves and SAPO-34 with a high yield (>90%) could be achieved at an accelerated crystallization rate [27]. It is distinct from the previous reports on the hydrothermal synthesis of SAPO-34 [15,16,19], implying that the aminothermal

* Corresponding author.
** Corresponding author.
E-mail addresses: tianpeng@dicp.ac.cn (P. Tian), liuzm@dicp.ac.cn (Z. Liu).
[1] These authors contributed equally to this work.

http://dx.doi.org/10.1016/j.micromeso.2017.04.035
1387-1811/

crystallization process of SAPO-34 may differ from the hydrothermal system.

Generally, investigation on the synthesis process of molecular sieves is conducive to understanding the crystallization mechanism and allows a rational design and synthesis of products with desired compositions and properties [28,29]. However, molecular sieves are usually synthesized from amorphous gels which are general inhomogeneous with both liquid and solid components under hydrothermal conditions. Numerous multiple-component reactions and equilibrium and condensation steps occur simultaneously, complicating the crystallization process and making the study on crystallization difficult [30–33]. So far, many efforts have been dedicated to understanding the crystallization mechanism of SAPO-34 [34–41]. Vistad et al. studied the hydrothermal crystallization of SAPO-34 with morpholine as a structure-directing agent in the presence of HF [42,43]. They demonstrated that the gel first dissolved into small units which condensed to no more than 4-rings (4R) and then a layered intermediate (the prephase) started to form. The next step was the redissolution of the prephase into 4R building units of different types and the subsequent nucleation and crystallization of triclinic SAPO-34. Our group have studied the crystallization and Si incorporation of SAPO-34 with triethylamine as the template and revealed that the crystal nuclei of SAPO-34 resulted from the structure rearrangement of the initial gel and the condensation of the hydroxyls [44]. About 80% of Si atoms directly took part in the formation of the crystal nuclei as well as in the growth of crystal grains in the earlier stage (<2.5 h). Afterwards, the relative content of Si in the product increased slightly with a little decrease of Al and P. Eventually, diverse Si environments appeared in the framework of SAPO-34. In our following study on the crystallization process of SAPO-34 templated by diethylamine, we further revealed a nonuniform Si distribution phenomenon in the SAPO-34 crystals with an increasing content from the core to the surface [16]. This finding is valuable for understanding the spatial distribution of Brønsted acid sites in the crystals, which is crucial for the catalytic applications of SAPO-34 [13,45,46]. Moreover, Huang and co-workers investigated the crystallization of SAPO-34 under dry gel conversion conditions including steam-assisted conversion (SAC) and vapor-phase transport (VPT) using diethylamine as the template [47]. They found that SAPO-34 crystallized from a semicrystalline precursor with a layered structure held mainly by weak nonbonding interaction. From the above literatures, it can be seen that the evolution of crystallization may vary with the synthetic methods (hydrothermal synthesis or dry-gel conversion), even though the organic template and product phase are the same.

In the present work, we examined the aminothermal synthesis process of SAPO-34 by using TEA as the solvent and template, aiming at better understanding the crystallization mechanism and elucidating the reason of the high solid yield and fast crystallization rate associated with this synthetic system. As a comparison, the hydrothermal synthesis of SAPO-34 with TEA as a template was also investigated. Many characterization methods were employed to follow the SAPO-34 crystallization including XRD, SEM, IR, UV-Raman, XRF and various solid-state NMR techniques.

2. Experimental section

2.1. Sample preparation

Organic amine used in the synthesis was triethylamine (TEA, 99.5 wt%). Pseudoboehmite (70.5 wt%), orthophosphoric acid (85 wt%), and silica sol (27.5 wt%, Shenyang Chemical Co. Ltd.) were used as inorganic precursors. All the chemicals were used without further purification.

SAPO-34 was aminothermally synthesized from a gel composition of 7.0TEA: $1.0Al_2O_3$: $0.9P_2O_5$: $0.3SiO_2$: $15.7H_2O$. A typical synthesis procedure was as follows. Organic amine, pseudoboehmite, silica sol and water were added in sequence into a glass beaker. The mixture was stirred at room temperature for 5 min, and then transferred into a 100 mL stainless steel autoclave. After further addition of phosphoric acid, the autoclave was sealed quickly, placed in an oven and rotated at 60 rpm for 30 min to get a homogeneous mixture. Subsequently, the autoclave was heated in 60 min to the 160 °C under rotation and kept for a certain time. The autoclaves were taken out from the oven periodically. The as-synthesized sample was separated by centrifugation and divided into two parts. One part was directly dried in air at room temperature, and the other part was washed with distilled water and dried in air. The crystallization time was recorded once the temperature of the oven reached 160 °C. Moreover, the initially mixed gel without heating was also characterized and named as 0 h(RT) sample. The solid yield of samples was calculated by the following formula: $\text{Yield}\ (\%) = M_{sample} \times 85\% \times 100/(M_{Al_2O_3+P_2O_5+SiO_2})_{gel}$, where M_{sample}, 85%, and $(M_{Al_2O_3+P_2O_5+SiO_2})_{gel}$ stand for the weight of solid sample, an estimated value of framework compounds included in the sample, and the dry mass of three inorganic oxides in the starting mixture, respectively. The relative crystallinity of the samples was calculated using the integrated intensities of the three strong characteristic diffraction peaks from XRD patterns after baseline correction by the following formula: relative crystallinity $(\%) = (I_1+I_2+I_3)_{sample}/(I_1+I_2+I_3)_{reference}$. I_1, I_2, I_3 stand for integrated intensities of the three peaks of 9.5°, 15.9°, and 20.6°. The 48 h sample obtained under aminothermal synthesis was used as the reference.

The starting molar ratio for the hydrothermal synthesis of SAPO-34 was 3.0TEA: $1.0Al_2O_3$: $0.9P_2O_5$: $0.3SiO_2$: 50 H_2O. Typically, the procedure was performed as follows: Pseudoboehmite, deionized water, phosphoric acid and silica sol were added in sequence into a glass beaker. The mixture was stirred at room temperature for 30 min. After further addition of organic amine, the mixture was transferred into a 100 mL stainless steel autoclave and placed in an oven and rotated at 60 rpm for 30 min to get a homogeneous mixture. Subsequently, the autoclave was heated in 60 min to the 160 °C under rotation and kept for a certain time. The as-synthesized sample was separated by centrifugation without washing and dried in air at room temperature. The crystallization time was recorded once the temperature of the oven reached 160 °C. The initially mixed gel without heating was named as HT-0h (RT).

2.2. Characterization

The powder XRD pattern was collected to determine the crystalline phase on a PANalytical X'Pert PRO X-ray diffractometer with Cu-Ka radiation ($\lambda = 1.54059$ Å) operated at 40 kV and 40 mA. The morphologies and the crystal sizes of the samples were observed by scanning electron microscopy (SEM, Hitachi 3000). The chemical composition of the samples was determined with a Philips Magix-601 X-ray fluorescence (XRF) spectrometer. IR spectra of the samples in the region of the framework stretching vibrations (400-4000 cm^{-1}) were measured using KBr containing pellets on a Bruker Tensor 27 spectrophotometer. UV Raman spectra were measured with a Jobin-YvonT64000 triple-stage spectrometer with spectral resolution of 2 cm^{-1}. The laser line at 325 nm of a He/Cd laser was used as an exciting source with an output of 50 mW. The power of the laser at the sample was about 3.0 mW.

All solid state NMR experiments were performed on a Bruker Avance III 600 spectrometer equipped with a 14.1 T wide-bore magnet. The resonance frequencies in this field strength were

156.4, 242.9 and 119.2 MHz for ^{27}Al, ^{31}P and ^{29}Si, respectively. A 4 mm MAS probe with a spinning rate of 13 kHz was employed to acquire ^{31}P and ^{27}Al NMR spectra. ^{27}Al MAS NMR spectra were acquired using a single pulse sequence. A 200 scans were accumulated with a $\pi/8$ pulse width of 0.75 μs and a recycle delay of 2 s. Chemical shifts were referenced to $(NH_4)Al(SO_4)_2 \cdot 12H_2O$ at −0.4 ppm. ^{31}P MAS NMR spectra were recorded using high-power proton decoupling. A 100 scans were accumulated with a $\pi/4$ pulse width of 2.25 μs and a 4 s recycle delay. Chemical shifts were referenced to 85% H_3PO_4 at 0 ppm. ^{29}Si MAS NMR spectrum was recorded with a 7 mm MAS probe with a spinning rate of 6 kHz using high-power proton decoupling. A 5000–6000 scans were accumulated with a $\pi/4$ pulse width of 2.5 μs and a 10 s recycle delay. Chemical shifts were referenced to 4,4-dimethyl-4-silapentane sulfonate sodium salt (DSS). ^{27}Al{^{31}P} REDOR experiments were performed with the 4.0 mm probe with a spinning speed of 10 kHz using the standard REDOR pulse sequence. The REDOR experiment is a rotor synchronized double resonance MAS technique. This technique involves two experiments with the first one being normal spin-echo experiment on ^{27}Al (observing nucleus). In the second (REDOR) experiment, during the spin−echo on ^{27}Al, a number of 180° pulses are applied to ^{31}P (dephasing nucleus). The echo intensity of REDOR experiments will decrease because of a nonzero average of dipolar coupling compared to the normal echo without 180° dephasing pulses. A 2.5-μs 90° pulse was also used for ^{27}Al. ^{31}P 180° dephasing pulse length was typical 11 μs.

3. Results and discussion

3.1. X-ray diffraction and morphology study of the samples with different crystallization durations

To monitor the evolution of long range ordering of the aminothermal gel, powder XRD patterns of the washed and unwashed as-synthesized samples with different crystallization time were recorded and given in Fig. 1. The pattern of the initial unwashed gel shows an obvious reflection at 8.7° together with several weak peaks, suggesting that the reorganization of amorphous gel occurs immediately upon mixing and results in the formation of an intermediate phase. The broad reflection and the intensity distribution (i.e., a strong reflection with a low 2θ value and a series of reflections in the middle and high 2θ regions) indicated a semicrystalline layer type material with a certain long-range ordering. Upon washing, these broad reflections disappear in the corresponding XRD pattern and only broad amorphous peaks indexed to unreacted pseudoboehmite could be observed (Fig. 1b), further implying that the intermediate phase is a soluble semicrystalline layered material probably held by the weak forces such as hydrogen bonding and vander Waals forces [38,41,47]. Heating the gel for 3 h, the intensity of the peaks due to the layered phase in the unwashed sample increases, while the amount of pseudoboehmite in the washed sample decreases sharply, indicating the rapid activation/transformation of pseudoboehmite source in the aminothermal environment. When the heating time is prolonged to 5 h, several fingerprint peaks associated with the CHA-type framework start to emerge. Upon washing, all broad reflections from the layered phase vanish completely, and only sharp diffraction peaks of SAPO-34 remain in the pattern (Fig. 1b). Meanwhile, the relative intensities of the peaks ascribed to the intermediate phase change slightly, indicating that the structure of this semicrystalline phase evolve with time and is likely accompanied by the slight rearrangement of the layered phase. Further heating the gel leads to the gradual increase of SAPO-34 in the unwashed samples at the expense of the semicrystalline layered phase. The fully crystalline SAPO-34 phase is obtained after heating for 24 h, and the intensities of the reflections increase gradually with time till the end of the experiments (48 h).

The crystallization curve based on the relative crystallinity of the washed samples is plotted in Fig. 2. It is in accordance with the

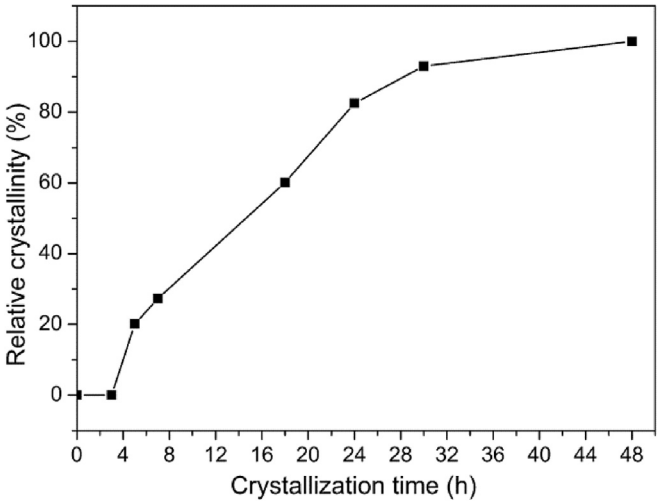

Fig. 2. The crystallization curve of SAPO-34 under aminothermal conditions.

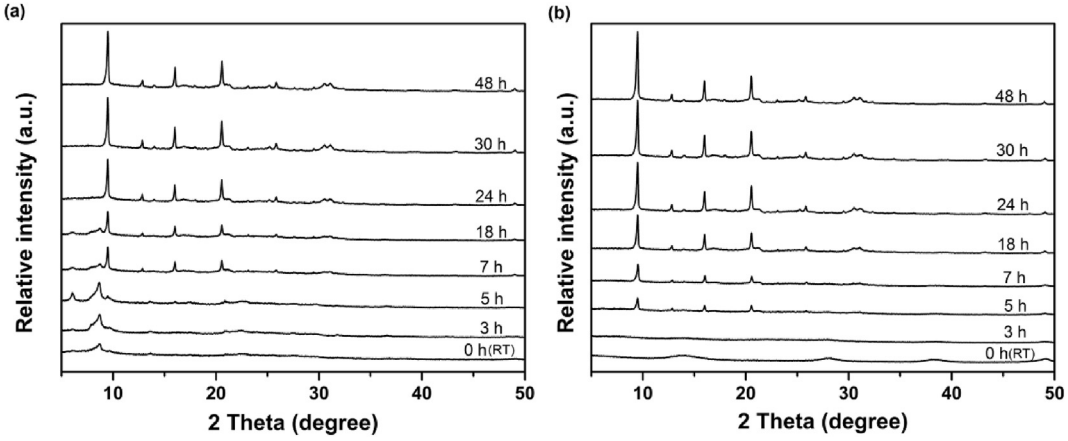

Fig. 1. XRD patterns of the unwashed (a) and washed (b) samples aminothermally synthesized with different crystallization durations.

S-shaped growth curve which is described as an induction period followed by a continuous crystal growth stage and a stable crystallization stage. The relative crystallinity of SAPO-34 rises with time and reaches 83% after heated for 24 h. Afterwards, the crystallinity of the samples rises slowly with time.

Fig. 3 gives the SEM images of the selected unwashed samples with different crystallization times. It can be seen that the initial gel and the 3 h sample mainly consist of irregular blocks, which implies the amorphous morphology of the layered phase. Cubic-like SAPO-34 crystals begin to appear on the surface of irregular particles after heating for 5 h, corresponding well to the XRD results. Further prolonging the crystallization time, the amorphous solids gradually transform into SAPO-34 crystals in the products. SEM images of the corresponding washed samples are shown in Fig. S1. Clearly, the crystal sizes grow with the evolution of crystallization and pure SAPO-34 crystals are observed in the washed products after 24 h.

3.2. Evolution of the chemical environments of the framework atoms in the samples studied by NMR

To investigate the local structural information of P, Al, and Si atoms in the solids with different crystallization durations, solid-state MAS NMR experiments were performed. Fig. 4a displays the ^{27}Al MAS NMR spectra of the unwashed samples, all of which show an intense peak at 42.4 ppm, assigned to tetrahedrally coordinated Al in local structures of $Al(OP)_4$. Additionally, the signal at 8.6 ppm

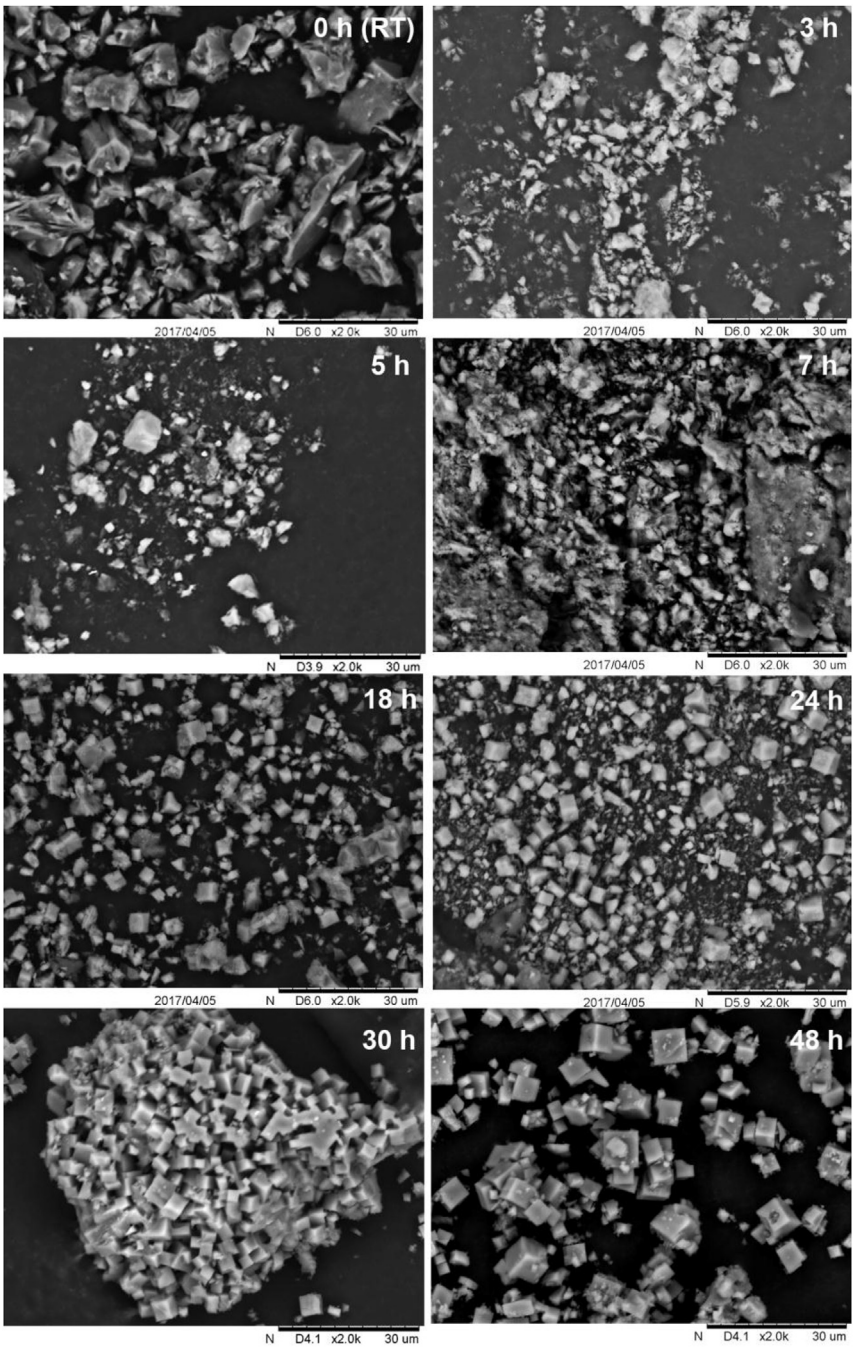

Fig. 3. SEM images of the unwashed samples synthesized with different crystallization durations.

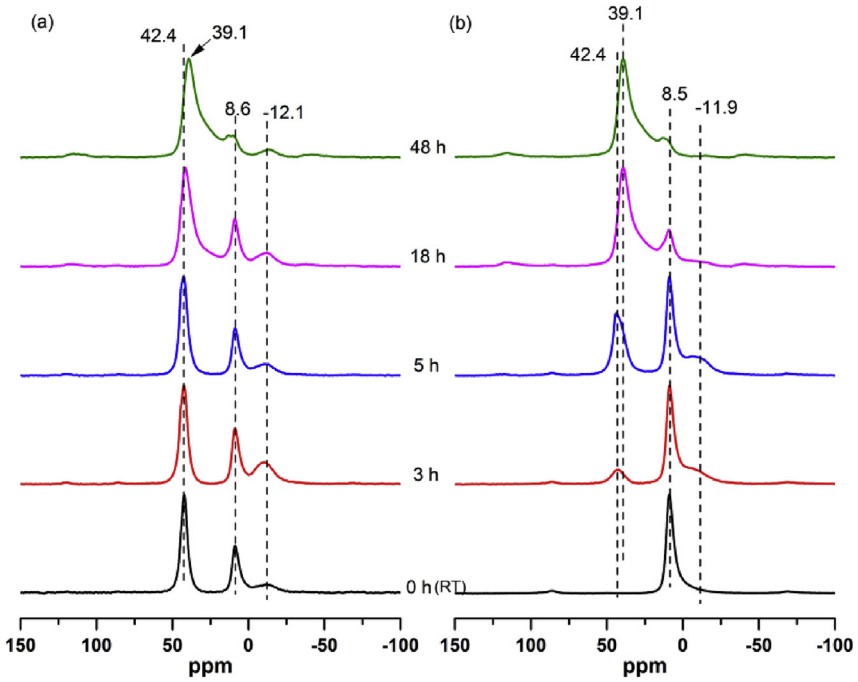

Fig. 4. ^{27}Al MAS NMR spectra of the unwashed (a) and washed (b) samples aminothermally synthesized with different crystallization durations.

is attributed to either unreacted alumina source or the penta-coordinated Al atoms formed by tetrahedral Al bonding with water or template, while the weak peak at −12.1 ppm indicates the presence of a small amount of octahedral Al atoms [48]. Throughout the process of crystallization, the spectra of the unwashed samples show a bit of difference, implying the slightly different chemical environment of Al atoms between the layered phase and SAPO-34 phase. However, obvious change occurs in the ^{27}Al spectra of the washed samples (Fig. 4b). For the initially washed sample without heating, only one strong peak at 8.5 ppm is observed in the spectrum, which is due to the unreacted alumina source as evidenced by XRD analysis. Notably, the signals at 42.4 and −12.1 ppm in the corresponding unwashed sample vanish, implying that the corresponding Al species are soluble, which should originate from the semicrystalline layered phase. After heating for 3 h, two weak signals at 42.4 ppm and −11.9 ppm related to insoluble tetrahedral and octahedral Al species start to appear in the ^{27}Al spectrum. Given that only broad weak peaks related to alumina source are detected in the XRD of the 3 h sample, these two Al species likely come from the newly formed AlPO phase with amorphous nature or very small crystalline size (<20 nm). Subsequently, the signal at 42.4 ppm becomes stronger at the expense of the signal at 8.5 ppm with increasing crystallization time, consistent with the formation of SAPO-34 and the depletion of alumina source. The ^{27}Al spectra of the samples with crystallization time longer than 18 h are similar to that reported for SAPO-34 [47]. Overall, the changes in the Al environments are in accordance with the XRD results.

The ^{31}P MAS NMR spectra of the samples synthesized at different crystallization times are shown in Fig. 5. The spectrum of the unwashed initial gel exhibits two peaks centered at around −19.3 and −29.1 ppm. Particularly, the sharp peak at −19.3 ppm disappears after washing, which should be attributed to the P atoms in the layered material in the form of $P(OAl)_x(OH)_y$ ($x < 4$). Its narrow peak width indicates the ordered local environment around P atoms, though they are not fully condensed. The broad peak at −13.8 ppm is assigned to the amorphous P species arise from the remaining H_3PO_4 in the gel or amorphous aluminophosphate. For the unwashed sample heated for 5 h, a small weak signal at −29.1 ppm is observed, which is assigned to the $P(OAl)_4$ species in the framework of SAPO-34 in combination with the XRD results. Afterwards, the intensity of the peak due to SAPO-34 increases at the expense of the signals at −13.8 and −19.3 ppm. Upon washing, the ^{31}P spectra of the samples show distinct changes except the 48 h sample (Fig. 5b), which is due to the dissolution of the layered material. For the initial raw mixtures, only a broad weak signal at −9.9 ppm associated with amorphous aluminophosphate is observed. After heating the mixtures for 3 h, an upfield shift of the broad peak from −9.9 to −15.9 ppm could be observed, which suggests the increased condensation degree of P species. Simultaneously, a weak shoulder at −29.1 ppm assigned to the $P(OAl)_4$ species appears, which is consistent with the existence of tetrahedral Al species in the corresponding ^{27}Al spectrum, indicating the formation of small amount of SAPO-34 nanocrystals though it is under the detection limit of XRD. After $t \geq 18$ h, only a signal around −29.1 ppm assigned to the tetrahedral P in the SAPO-34 is observed in the spectra of the washed samples, indicating their full crystallization.

To further identify the connectivity between the Al and P atoms in the unwashed samples, ^{27}Al{^{31}P} REDOR experiments were carried out to make a clear assignment of signals in the Al spectra (Fig. 6). For the 0 h unwashed sample, two peaks at 42.2 and −12.1 ppm are observed in the REDOR difference spectrum (**Δ**S), suggesting that both the tetrahedral and octahedral Al atoms have close vicinity with the ^{31}P nuclei. Considering that these two Al species exist in the semicrystalline layered phase, the layered precursor should contain Al species in the form of $Al(OP)_4$ and $Al(OP)_4(H_2O)_x(TEA)_y$ ($x + y = 2$, $x \geq 1$). The absence of the signal at 8.8 ppm in the REDOR difference spectra implies that the corresponding Al species originate from unreacted alumina source. In the REDOR difference spectrum of the 18 h heated sample, all of the three peaks exist except a decrease of the peak at 9.0 ppm, implying the existence of some unreacted alumina at this time. After heating for 48 h, the REDOR difference spectrum of the unwashed sample is

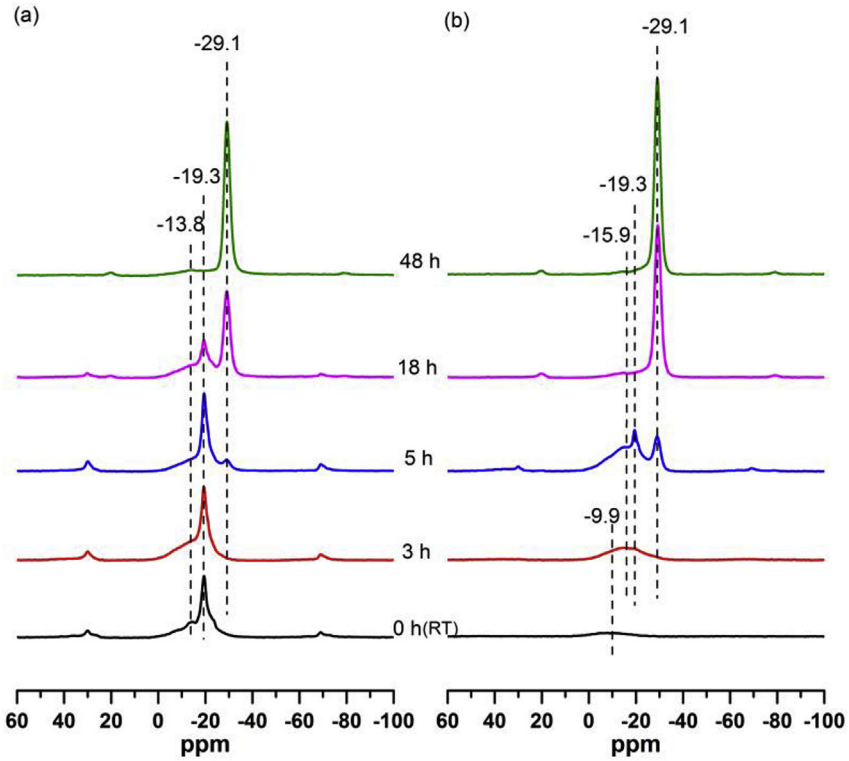

Fig. 5. ^{31}P MAS NMR spectra of the unwashed (a) and washed (b) samples aminothermally synthesized with different crystallization durations.

proximate to the corresponding ^{27}Al spectrum, confirming the good connectivity with ^{31}P nuclei of the three Al species and their origin from SAPO-34.

The ^{29}Si MAS NMR spectra of the unwashed and washed samples are displayed in Fig. 7. Only a broad peak around −110.9 ppm is observed in the ^{29}Si spectrum of the initial gel, which can be assigned to unreacted amorphous silica mainly with $Si(OSi)_4$ environments. Since the semicrystalline layered phase has already formed in the raw mixture and the Al and P atoms in the layered material are proved to have ordered microenvironments and sharp NMR resonances, the broaden peak in the ^{29}Si spectrum here indicates that the layered material is Si-free or Si-deficient. The spectrum of the unwashed 5 h sample shows a small peak centered at −92.0 ppm, which becomes more apparent after washing, indicating the generation of $Si(OAl)_4$ in the sample. As a small amount of SAPO-34 has already formed after heating for 3 h as revealed by the ^{27}Al and ^{31}P spectra, it is supposed that Si atoms have directly participated in the formation of SAPO-34 at the initial crystallization stage. Moreover, several weak peaks (−80 to −92 ppm) which correspond to $Si(OAl)_n(OH)_{(4-n)}$ (n = 2, 3) species also emerge in the spectra, implying the formation of a small amount of amorphous aluminosilicate particles due to the reaction of silica with alumina. Further heating the gel, the intensities of the peaks from amorphous silica and aluminosilicate species decrease, whereas the

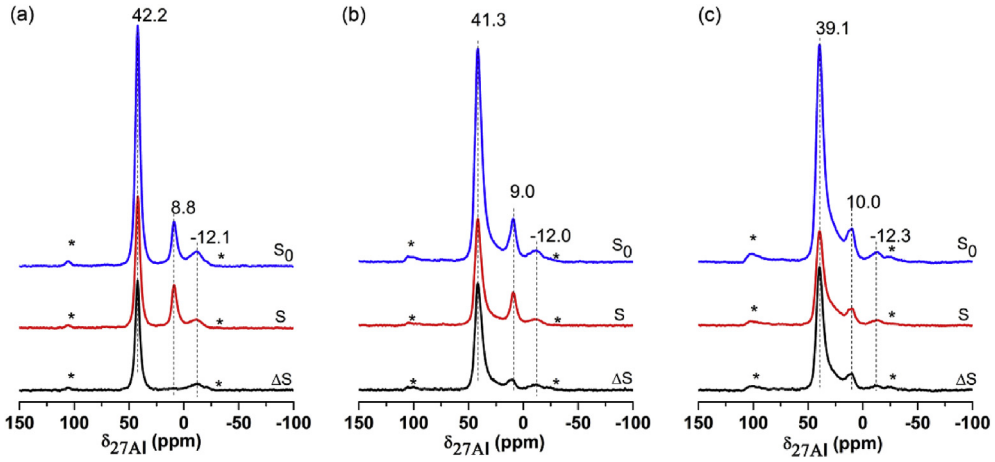

Fig. 6. ^{27}Al {^{31}P} REDOR spectra of the 0 h (RT) (a), 18 h (b), and 48 h (c) unwashed samples (S_0: ^{27}Al spin-echo, S: REDOR, ΔS: REDOR difference. Asterisks indicate spinning sidebands.).

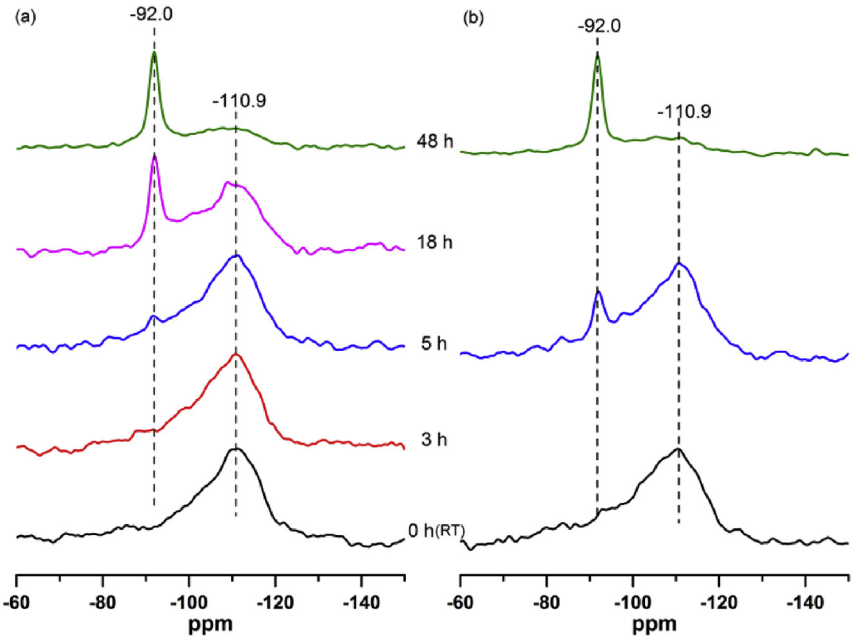

Fig. 7. ^{29}Si MAS NMR spectra of the unwashed (a) and washed (b) samples aminothermally synthesized with different crystallization durations.

amount of the $Si(OAl)_4$ species increase, showing that more Si atoms incorporate into the framework of SAPO-34. At the end of the crystallization, the spectra of the samples present a strong peak at −92.0 ppm, indicating the dominant existence of $Si(OAl)_4$ species in the SAPO-34 product [48].

3.3. FT-IR study of the samples with different crystallization durations

FT-IR spectra of the selected unwashed samples are shown in Fig. 8. The framework characteristic vibration peaks of the 48 h sample are comparable to the SAPO-34 reported in the literature [44]. The bands are assigned as follows: 3650-3000 cm^{-1} arising from the hydroxyl vibration; 1300-1000 cm^{-1} ascribed to the asymmetric stretch of T-O tetrahedra; 740 cm^{-1} due to the symmetric stretch of T-O tetrahedra; the bands below 700 cm^{-1} corresponding to the vibration of double-6 rings (D6R) and the bending of T-O. Moreover, small bands at 1400, 1480, 2734 and 2935 cm^{-1} could be observed, which arise from the $-CH_2$ and $-CH_3$ groups of the template.

By comparing the IR spectra of the samples, it can be seen that two bands at 2493 and 2677 cm^{-1} appear in all the spectra except for that of the 48 h sample, which are ascribed to the P-containing groups in H_3PO_4 or amorphous aluminophosphate, in consistent with the above NMR characterization. In addition, the broad stretch bands (3000−3650 cm^{-1}) of the hydroxyls gradually weaken with time, suggesting the structure rearrangement and the condensation of hydroxyl groups occur during the progress of the crystallization. Another interesting phenomenon is that the band at 635 cm^{-1} associated with the D6R units emerges even in the initial gel. In combination with the above results, we speculate that the D6R should originate from the semicrystalline layered phase [47]. To further confirm our speculation, FT-IR spectra of the washed samples are also measured and shown in Fig. S2. It can be seen that the band at 635 cm^{-1} vanishes after washing, indicating that the D6Rs are removed from the gel along with the dissolution of the semicrystalline layered phase.

3.4. Crystallization of SAPO-34 under hydrothermal conditions

To better understand the aminothermal crystallization process, we further investigate the hydrothermal crystallization process of SAPO-34 with TEA as the template at 160 °C. The XRD patterns of

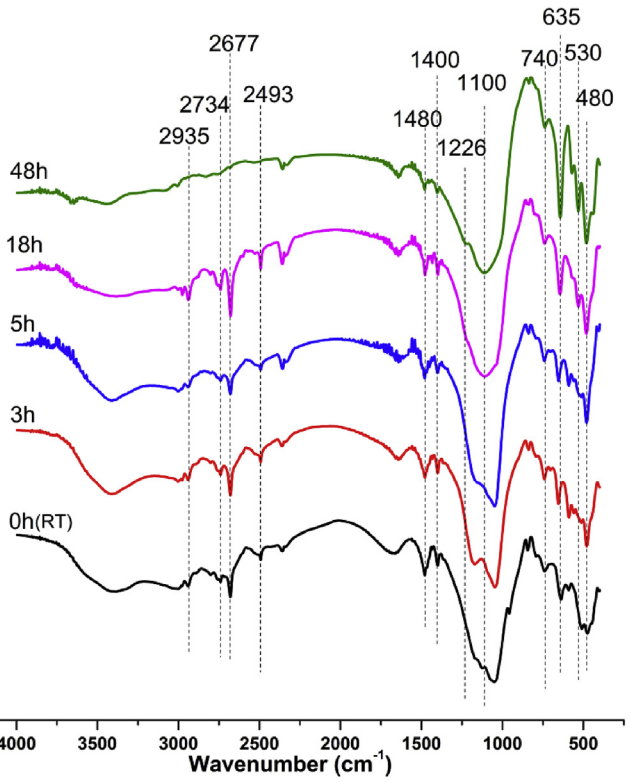

Fig. 8. FT-IR spectra of the unwashed samples aminothermally synthesized with different crystallization durations.

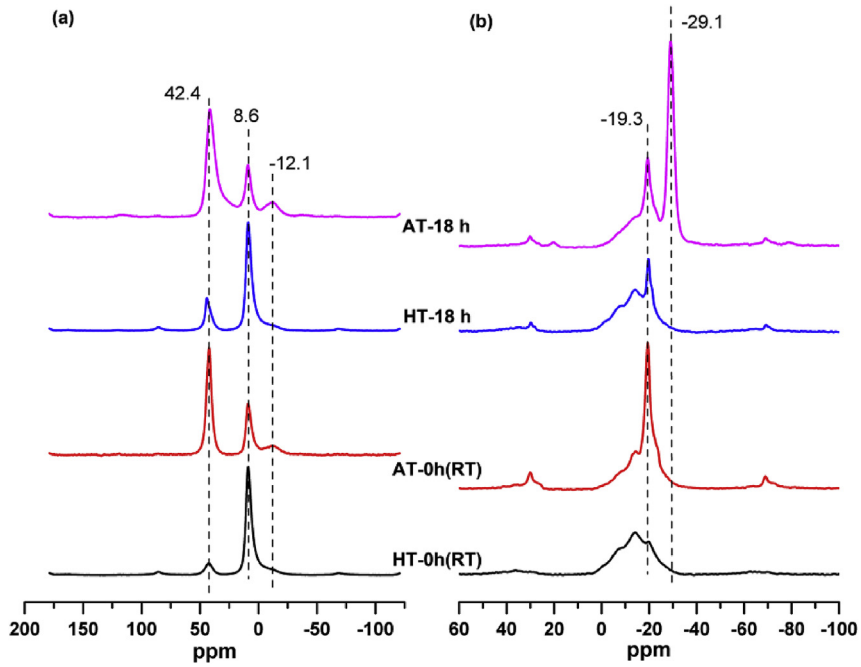

Fig. 9. ^{27}Al (a) and ^{31}P MAS NMR (b) spectra of the 0 h and 18 h unwashed samples synthesized via hydrothermal and aminothermal method.

the unwashed products from hydrothermal synthesis with durations from 0 to 48 h are given in Fig. S3. It can be seen that the pattern of the unwashed initial gel is similar to that of pseudoboehmite, which differs obviously from the aminothermal synthesis process where semicrystalline layered phase forms immediately after the raw materials are mixed. Heating the gel for 18 h, several weak peaks together with broad reflections from pseudoboehmite appear and become more obvious at 24 h, which could be attributed to the formation of semicrystalline layered phase. No reflections from SAPO-34 could be discerned at this time. Clearly, the crystallization rate of SAPO-34 under hydrothermal system is much slower than that of the aminothermal process. Meanwhile, the solid yield of hydrothermal process after 48 h (46.8%) is lower than that of the aminothermal process (90.4%). Further prolonging the hydrothermal crystallization time to 96 h, the solid yield doesn't increase much due to the large water amount that causes the loss of inorganic sources and thus a lower yield.

Fig. 9 shows the ^{27}Al and ^{31}P spectra of the unwashed hydrothermal samples heated for 0 h and 18 h (designated as HT-0h (RT) and HT-18 h). The corresponding spectra of the aminothermal samples (designated as AT-0h (RT) and AT-18 h) are also given to facilitate comparison. The ^{27}Al spectrum of the initial hydrothermal gel exhibits two peaks centered at 42.1 (weak) and 8.6 ppm (strong), arising from the tetra- and penta-coordinated Al species, respectively. As the crystallization time increases to 18 h, the peak due to the tetrahedral Al species grows stronger, corresponding to the formation of semicrystalline layered phase. However, the amount of tetrahedral Al species in HT-18 h is even lower than in the 0 h aminothermal sample. A similar phenomenon is also observed for the ^{31}P spectra. The content of partially condensed P atoms with signal at −19.3 ppm ($P(OAl)_x(OH)_y$, $x < 4$) in HT-18 h is lower than that in AT-0h (RT). More than half of the P atoms in HT-18 h sample exist in the form of amorphous aluminophosphate. The above results confirm that the aminothermal environment could promote the activation of Al source and its reactivity with P source.

UV Raman spectroscopy excited with 325 nm was employed to probe the host-guest interactions between template and framework [49]. The Raman bands in Fig. 10 have been well assigned in the literature [34]: the band at 355 cm^{-1} corresponds to the vibrational modes of isolated octahedral AlO_6 species originating from pseudoboehmite; the peak at 899 cm^{-1} is assigned to the symmetric stretching vibration of $P(OH)_3$ in phosphates; the bands at 740, 1016, 1036 and 1071 cm^{-1} are characteristics of the protonated TEA template; the bands at 472 and 1121 cm^{-1} are due to the framework vibration of well-crystallized products.

The Raman spectrum of the initial hydrothermal sample shows a strong band at 355 cm^{-1} that decreases significantly in intensity with the prolonged synthesis time. However, this band is very weak in the spectrum of the initial aminothermal mixture. The result further confirmed that alumina source is more reactive in the aminothermal environment than that in hydrothermal environment [50]. The bands at 1016 and 1035 cm^{-1}, which are assigned to the stretching modes of the C—C bond of the three ethyl chains attached to the protonated nitrogen atom of the amine, are present in the spectra of all samples, suggesting that the amine has been captured in the solids since the mixing of the initial gel. A previous study has demonstrated that the intensity of these two bands are sensitive to the surrounding environment and constrained TEA^+ ions would show a decreased intensity at 1016 and 1035 cm^{-1}.[32] On the other hand, the band at 1071 cm^{-1} arising from the vibration of C—N of the template is less affected by the external environment. This means that the intensity ratio of 1071 to 1016 (1035) cm^{-1} could be used to probe the local environment of the template (the band at 1071 cm^{-1} serves as an internal standard) [34]. Interestingly, the spectra of all aminothermal samples exhibit an obvious strong band at 1071 cm^{-1} and two weak bands at 1016 and 1035 cm^{-1}, while similar spectra are only observed for the hydrothermal samples with crystallization time of $t \geq 24$ h. These results show that intense interactions between TEA^+ ions and inorganic species exist in the aminothermal samples, and an ordered structure with entrapped TEA^+ ions was already formed at the initial stage under the aminothermal environment. The result is consistent with the XRD results and implies that the layered intermediates are organic-inorganic assembly.

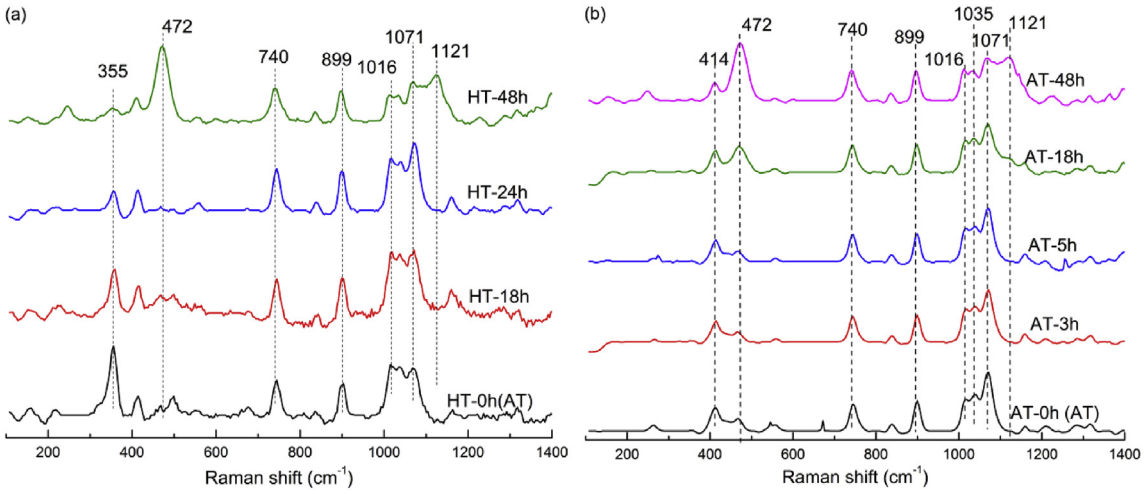

Fig. 10. UV Raman spectra of the unwashed samples synthesized via hydrothermal (a) and aminothermal methods (b).

3.5. *Crystallization mechanism of SAPO-34 under aminothermal conditions*

According to the above characterization, the aminothermal crystallization process of SAPO-34 can be proposed and depicted in Scheme 1. In the initial stage of crystallization, an AlPO prephase that consists of semicrystalline layered structure held together by weak nonbonding interactions forms immediately upon mixing Al and P and Si sources as well as TEA. It is supposed that the intense interactions between TEA^+ and inorganic species under aminothermal environment facilitate the formation and assembly of the layered phase, which further promotes the fast activation/depolymerization of Al source and thus the generation of large amount of Al—O—P bonds. A previous study suggests that the layered phase formed during the crystallization of SAPO-34 bears a resemblance to the (001) face of SAPO-34 in that it contains titled D6Rs and the D6R is energetically stable to terminate the structure of SAPO-34 on the (001) crystal surface [47]. Based on the above results, a possible structure of the layer material is given in Fig. S4. As can be seen, the structure consists of AlPO layers with D6R separated/stabilized by TEA^+, in which the Al species exist in tetrahedral form and $Al(O\text{-}P)_4(H_2O)_x(TEA)_y$ ($x + y = 2$, $x \geq 1$), and P species exist as not fully condensed $P(OAl)_x(OH)_y$ ($x + y = 4$, $x < 4$). It is noted that the lamellar structure is slightly variable as deduced from the slight alteration of the XRD patterns of the layered phase over time. Besides, small amount of unreacted alumina, amorphous AlPO and SiO_2 coexist in the initial solid phase. Along with the crystallization, SAPO-34 starts to emerge at 3 h though it is invisible for XRD. In combination with the ^{29}Si spectra which show the formation of $Si(OAl)_4$ species in the early crystallization stage, we speculate that Si directly participates in the formation of SAPO-34 framework. Subsequently, the content of SAPO-34 in the solids increases and becomes XRD detectable at 5 h. Its relative crystallinity rises with time at the expense of layered phase. Considering the difference in Si element between layered phase and SAPO-34, SAPO-34 may nucleate from the rearrangement of the D6R in the semicrystalline layered phase through bond breaking, reforming and Si incorporation. Since 24 h, the layered phase disappears and amorphous material becomes less and less. The nutrition for the growth of SAPO-34 (Al, P, and Si elements) should mainly come from the liquid. The solid yield and crystallinity of SAPO-34 increase with time until the end of the crystallization. Regarding the corresponding hydrothermal process, the interaction between TEA^+ ions and inorganic species is relatively weak and the semicrystalline layered structure is hardly formed until $t \geq 18$ h, which is possibly due to the low stability of the layered structure in the hydrothermal system with a large amount of water. Also, the semicrystalline layered structure is not stable in the hydrothermal system with a large amount of water. Therefore, the activation of alumina source is slow and the nucleation induction period of the hydrothermal

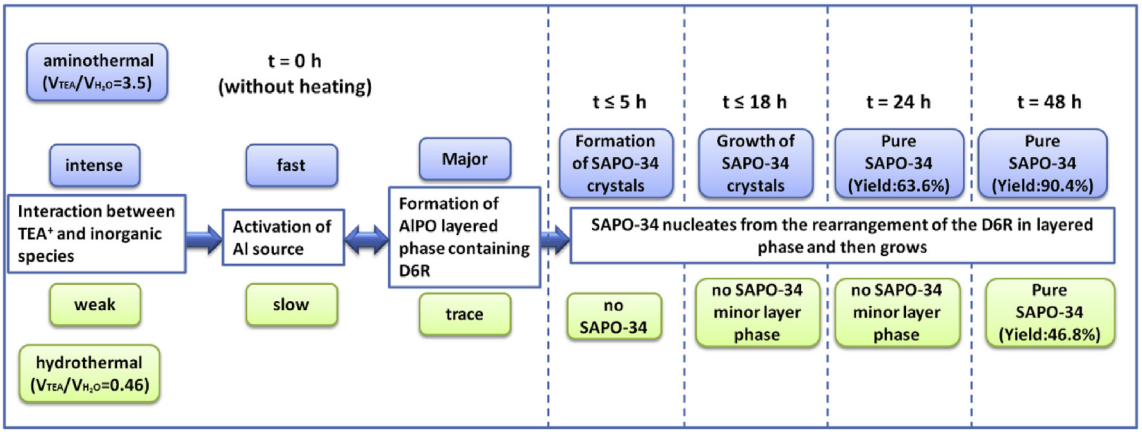

Scheme 1. Illustration of the crystallization process of SAPO-34 under aminothermal conditions at 160 °C and its comparison with the crystallization under hydrothermal system.

system is significantly prolonged and the crystallization process slows down.

4. Conclusions

In this work, the aminothermal crystallization process of SAPO-34 has been examined and compared with the hydrothermal process. The results clearly show that the intense interactions between TEA^+ and inorganic species under aminothermal environment facilitate the formation and assembly of a AlPO layered phase, which further accelerate the activation/depolymerization of Al source and the generation of large amount of Al–O–P bonds. The semicrystalline layered structure stabilized by TEA^+ is water-soluble, which plays an essential role in the formation of SAPO-34. SAPO-34 is likely to nucleate and grow from the rearrangement of the D6R in the layered phase through bond breaking, reforming and Si incorporation. The ^{29}Si spectra confirm that Si directly incorporates into the framework in the initial crystallization. At the latter stage of crystallization ($t \geq 24$ h), the nutrition for the growth of SAPO-34, such as Al, P, and Si elements, mainly comes from the liquid and finally a solid yield of 90.4% is achieved. For the hydrothermal process, the interactions between TEA^+ ions and inorganic species are relatively weak and the formation of the semicrystalline layered structure in the gel is difficult due to its low stability in the water. As a consequence, the activation of alumina source is slow and the formation of SAPO-34 is retarded, which appears after 24 h and achieves a solid yield of 46.8% at 48 h.

Acknowledgements

We would like to thank the financial support from National Natural Science Foundation of China (No. 21676262) and Key Research Program of Frontier Sciences, Chinese Academy of Sciences (Grant No. QYZDB-SSW-JSC040).

Appendix A. Supplementary data

Supplementary data related to this article can be found at http://dx.doi.org/10.1016/j.micromeso.2017.04.035.

References

[1] D.W. Breck, Zeolite Molecular Sieves: Structure, Chemistry and Use, Wiley, New York, 1974.
[2] A. Corma, Chem. Rev. 97 (1997) 2373–2420.
[3] E.M. Flanigen, in: E.M.F.H. van Bekkum, J.C. Jansen (Eds.), Stud. Surf. Sci. Catal, Elsevier, 1991, pp. 13–34.
[4] C.T. Kresge, W.J. Roth, Chem. Soc. Rev. 42 (2013) 3663–3670.
[5] B.M. Weckhuysen, J. Yu, Chem. Soc. Rev. 44 (2015) 7022–7024.
[6] B.M. Lok, C.A. Messina, R.L. Patton, R.T. Gajek, T.R. Cannan, E.M. Flanigen, J. Am. Chem. Soc. 106 (1984) 6092–6093.
[7] T. Cannan, E. Flanigen, R. Gajek, B. Lok, C. Messina, R. Patton, US Pat, 4440871 (1984).
[8] J. Liang, H. Li, S. Zhao, W. Guo, R. Wang, M. Ying, Appl. Catal. 64 (1990) 31–40.
[9] M. Stöcker, Microporous Mesoporous Mater 29 (1999) 3–48.
[10] W. Dai, G. Wu, L. Li, N. Guan, M. Hunger, Acs. Catal. 3 (2013) 588–596.
[11] Q. Sun, N. Wang, D. Xi, M. Yang, J. Yu, Chem. Commun. 50 (2014) 6502–6505.
[12] S. Wilson, P. Barger, Microporous Mesoporous Mater 29 (1999) 117–126.
[13] P. Tian, Y. Wei, M. Ye, Z. Liu, ACS. Catal. 5 (2015) 1922–1938.
[14] D. Fan, P. Tian, S. Xu, D. Wang, Y. Yang, J. Li, Q. Wang, M. Yang, Z. Liu, New J. Chem. 40 (2016) 4236–4244.
[15] E. Dumitriu, A. Azzouz, V. Hulea, D. Lutic, H. Kessler, Microporous Mater 10 (1997) 1–12.
[16] G. Liu, P. Tian, Y. Zhang, J. Li, L. Xu, S. Meng, Z. Liu, Microporous Mesoporous Mater 114 (2008) 416–423.
[17] A.M. Prakash, S. Unnikrishnan, J. Chem. Soc. Faraday Trans. 90 (1994) 2291–2296.
[18] N. Rajić, D. Stojaković, S. Hoçevar, V. Kaučič, Zeolites 13 (1993) 384–387.
[19] Y. Xu, P.J. Maddox, J.W. Couves, J. Chem. Soc. Faraday Trans. 86 (1990) 425–429.
[20] Y. Hirota, K. Murata, S. Tanaka, N. Nishiyama, Y. Egashira, K. Ueyama, Mater. Chem. Phys. 123 (2010) 507–509.
[21] H. Yang, Z. Liu, H. Gao, Z. Xie, J. Mater. Chem. 20 (2010) 3227–3231.
[22] L. Zhang, J. Yao, C. Zeng, N. Xu, Chem. Commun. (2003) 2232–2233.
[23] Y.Y. Jin, Q. Sun, G.D. Qi, C.G. Yang, J. Xu, F. Chen, X.J. Meng, F. Deng, F.S. Xiao, Angew. Chem. Int. Ed. 52 (2013) 9172–9175.
[24] J. Li, A. Corma, J. Yu, Chem. Soc. Rev. 44 (2015) 7112–7127.
[25] J. Hennessy, Zeolites: a synthetic solution, Nat. Mater 15 (2016), 6-6.
[26] D. Fan, P. Tian, S. Xu, Q. Xia, X. Su, L. Zhang, Y. Zhang, Y. He, Z. Liu, J. Mater. Chem. 22 (2012) 6568–6574.
[27] D. Fan, P. Tian, X. Su, Y. Yuan, D. Wang, C. Wang, M. Yang, L. Wang, S. Xu, Z. Liu, J. Mater. Chem. A 1 (2013) 14206–14213.
[28] M.B. Park, N.H. Ahn, R.W. Broach, C.P. Nicholas, G.J. Lewis, S.B. Hong, Chem. Mater 27 (2015) 1574–1582.
[29] T. Ikuno, W. Chaikittisilp, Z. Liu, T. Iida, Y. Yanaba, T. Yoshikawa, S. Kohara, T. Wakihara, T. Okubo, J. Am. Chem. Soc. 137 (2015) 14533–14544.
[30] V.P. Valtchev, K.N. Bozhilov, J. Phys. Chem. B 108 (2004) 15587–15598.
[31] P. Norby, Curr. Opin. Colloid In. 11 (2006) 118–125.
[32] J. Grand, H. Awala, S. Mintova, CrystEngComm 18 (2016) 650–664.
[33] G. Feng, P. Cheng, W. Yan, M. Boronat, X. Li, J.H. Su, J. Wang, Y. Li, A. Corma, R. Xu, J. Yu, Science 351 (2016) 1188–1191.
[34] F. Fan, Z. Feng, K. Sun, M. Guo, Q. Guo, Y. Song, W. Li, C. Li, Angew. Chem. Int. Ed. 48 (2009) 8743–8747.
[35] Z. Liu, W. Xu, G. Yang, R. Xu, Microporous Mesoporous Mater 22 (1998) 33–41.
[36] J. Xu, L. Chen, D. Zeng, J. Yang, M. Zhang, C. Ye, F. Deng, J. Phys. Chem. B 111 (2007) 7105–7113.
[37] J.G. Longstaffe, B. Chen, Y. Huang, Microporous Mesoporous Mater 98 (2007) 21–28.
[38] B. Chen, C.W. Kirby, Y. Huang, J. Phys. Chem. C 113 (2009) 15868–15876.
[39] B. Chen, Y. Huang, J. Phys. Chem. C 111 (2007) 15236–15243.
[40] Y. Huang, B.A. Demko, C.W. Kirby, Chem. Mater 15 (2003) 2437–2444.
[41] P. Tian, B. Li, S. Xu, X. Su, D. Wang, L. Zhang, D. Fan, Y. Qi, Z. Liu, J. Phys. Chem. C 117 (2013) 4048–4056.
[42] Ø.B. Vistad, E.W. Hansen, D.E. Akporiaye, K.P. Lillerud, J. Phys. Chem. A 103 (1999) 2540–2552.
[43] Ø.B. Vistad, D.E. Akporiaye, F. Taulelle, K.P. Lillerud, Chem. Mater 15 (2003) 1639–1649.
[44] J. Tan, Z. Liu, X. Bao, X. Liu, X. Han, C. He, R. Zhai, Microporous Mesoporous Mater 53 (2002) 97–108.
[45] M. Yang, P. Tian, C. Wang, Y. Yuan, Y. Yang, S. Xu, Y. He, Z. Liu, Chem. Commun. 50 (2014) 1845–1847.
[46] D. Fan, P. Tian, S. Xu, D. Wang, Y. Yang, J. Li, Q. Wang, M. Yang, Z. Liu, New J. Chem. 40 (2016) 4236–4244.
[47] L. Zhang, J. Bates, D. Chen, H.-Y. Nie, Y. Huang, J. Phys. Chem. C 115 (2011) 22309–22319.
[48] C.S. Blackwell, R.L. Patton, J. Phys. Chem. 92 (1988) 3965–3970.
[49] L. Marchese, A. Frache, E. Gianotti, G. Martra, M. Causà, S. Coluccia, Microporous Mesoporous Mater 30 (1999) 145–153.
[50] D. Grandjean, A.M. Beale, A.V. Petukhov, B.M. Weckhuysen, J. Am. Chem. Soc. 127 (2005) 14454–14465.